

Photodetachment studies of extended excited states in I^-Xe_n clusters ($n=1-54$)

Israella Becker and Ori Cheshnovsky

School of Chemistry, The Sackler Faculty of Exact Sciences, Tel-Aviv University, 69978 Tel-Aviv, Israel

(Received 2 December 1998; accepted 4 January 1999)

We present a comprehensive experimental study of bound excited states in I^-Xe_n clusters ($n=1-54$), using photoelectron spectroscopy and energy-dependent action spectroscopy. Starting at $n=4$, the electron detachment action spectra developed peaks lying in energy lower than the vertical binding energy. This behavior has been shown for both final spin states of the neutral iodine. It indicates the existence of bound electronic states extended over the xenon cluster. The peaks lying in energy below the $J=1/2$ detachment continuum of the iodine ($n>4$) were detected over the whole cluster size range of I^-Xe_n using electron detachment action spectroscopy. For the bound states relating to the $J=3/2$ continuum, in the size range $n=4-12$, thermionic emission has marked the existence of bound states. For $n>12$, these states were stabilized and detected via two-photon excitations. The picture, unveiled from the above photoelectron and action spectra, is the gradual evolution of bound excited states on the xenon solvent cluster. The critical size for the binding of an excited electron is $n=4$. At the largest cluster interrogated, I^-Xe_{54} , the binding energy amounts to 170 meV. We compare these states to the ground electronic state of Xe_n^- clusters, and discuss the differences between the experiments and model calculations. © 1999 American Institute of Physics. [S0021-9606(99)00913-7]

I. INTRODUCTION

Monomer closed-shell atoms and many molecules do not exhibit affinity to excess electrons, due to the efficient screening of the positive core by the closed shell. In the condensed form, however, many of these systems exhibit positive electron affinity (EA): While a single water molecule or ground-state noble gas atoms do not bind electrons, electrons are solvated in bulk water¹ and rare gas liquids and solids² (i.e., the bottom of the conduction band of solid xenon lies ~ 0.58 eV below the vacuum level).

Inspired by these facts, the phenomenon of excess electrons solvated in clusters has attracted scientists over the last two decades. A considerable amount of experimental and theoretical efforts has been invested in exploring systems for which a stable anionic monomer does *not* exist, such as molecular $(CO_2)_n^-$ (Refs. 3–5), $(NH_3)_n$ (Ref. 6), and $(H_2O)_n$ (Ref. 7), and atomic He_n^- (Ref. 8), Ne_n^- (Ref. 9), and Xe_n^- (Ref. 10) clusters.

Unlike molecular clusters, where the interactions between the solvating molecules, and consequently between them and the solvated electron, are strongly affected by the complex intermolecular interactions, the binding of excess electrons to rare gas atoms is solely due to the collective polarization of the surrounding solvating atoms, which makes it the simplest excess electron system to investigate. The focus of this study is the binding of excess electrons in xenon clusters.

Two groups performed theoretical calculations,^{11,12} predicting the minimal xenon cluster size to bind an electron to be 6–7 atoms; Martyna and Berne¹¹ applied diffusion Monte Carlo simulations using a pair-polarization model, and showed that an electron would attach to a cluster as small as

Xe_6 . Further calculations, taking into account many-body polarization interactions, found that Xe_7 was the smallest cluster to bind an electron. Stampfli and Bennemann¹² proposed a dielectric continuum model to calculate the EA of small rare gas clusters, and determined the critical cluster size to be Xe_6-Xe_9 . The experimental evidence for the existence of stable Xe_n^- was provided by Haberland and co-workers.¹⁰ The existence of small Xe_n^- has been unambiguously demonstrated; yet, the critical cluster size for electron binding in the ground-state cluster was inconclusive ($n=6$ or smaller), due to the possible presence of electronically metastable Xe_n^- . In these experiments, the very low concentrations of clusters, resulting from their low electron binding energy, prevented further spectroscopic studies.

Recently, Becker, Markovich, and Cheshnovsky (BMC) have introduced a new experimental approach to study the evolution of bound excess electron states in xenon clusters, by using I^-Xe_n clusters¹³ (we will refer to Ref. 13 as BMC throughout the current paper). It is based on the fact that the electron, localized on the solvated anion, can be photoexcited only to the extended states in the xenon-iodine cluster, since the bare iodine anion does not support any bound excited states. Practically, we use the anionic electron as an internal electron source, assuming that the excited states of the I^-Xe_n clusters highly resemble the ground state of the Xe_n^- clusters.¹⁴

This approach has two distinct advantages. First, due to high EA (>3 eV) these clusters can be generated in large quantities. Second, both bound and unbound electron states in the xenon clusters are accessible via excitation from the deeply bound impurity state. Figure 1 depicts the principles of our experimental strategy: High energy photons $h\nu_1$

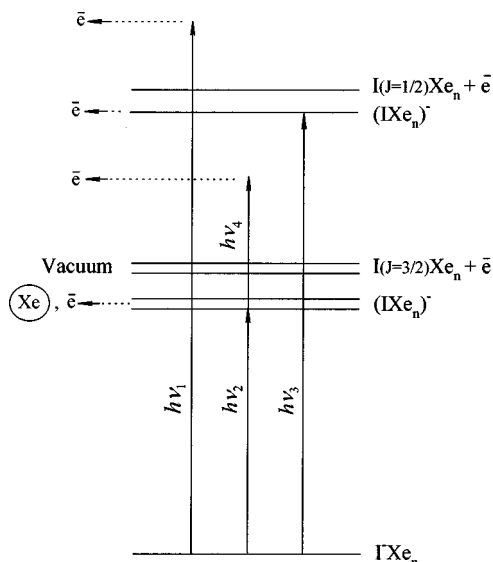


FIG. 1. A scheme of the excited states of the Γ^-Xe_n clusters and the photoinduced processes following various excitation schemes: $h\nu_1$ denotes the direct photodetachment process; $h\nu_2$ is excitation to the two bound $(IXe_n)^-$ states which lie below the almost degenerate two $J=3/2$ states of the neutral iodine, from which an electron or a xenon atom can be thermally emitted. The bound excited states can be further excited ($h\nu_4$) to a detachment continuum. $h\nu_3$ stands for the excitation to the autodetachment $(IXe_n)^-$ resonance lying below the $J=1/2$ of the neutral iodine.

($h\nu_1 > EA$), are used to measure the vertical binding energy of the anionic electron to the cluster via photoelectron spectroscopy (PES). Lower energy photons, $h\nu_2$ and $h\nu_3$, are used to excite the electron to the extended states of the xenon solvent. The excitation to bound or to autodetaching states is monitored by recording the yield of spontaneously emitted electrons and photofragments, or by subsequently detaching the excited bound electron with $h\nu_4$ photons. The generic name "action spectroscopy" is given to the above methods in which the energy dependence of the photoinduced processes is monitored. The difference between the vertical binding energy in each mass-selected cluster and the corresponding excitation energy is the binding energy of the excess electron to a xenon cluster. This methodology is quite general for the investigation of empty bands in clusters, via the excitation of slightly perturbing impurity states. It is versatile and can be adapted to the characterization of states residing above or below the vacuum level, by using different detection schemes.

As we have already emphasized,¹³ the analogy to the bare xenon clusters is incomplete. In our Γ^-Xe_n experiment, the conduction band of the bare xenon cluster is perturbed by the presence of the iodine core, at least in small clusters. Also, note that in the vertical photoexcitation process, non-relaxed geometries of the xenon clusters are accessed, with no direct measurement of the adiabatic binding energies.

Anion impurities embedded in rare gas clusters have been previously studied.^{15,16} These studies focused on the impurity ground-state properties. The focal point of BMC and the present work is the investigation of the extended

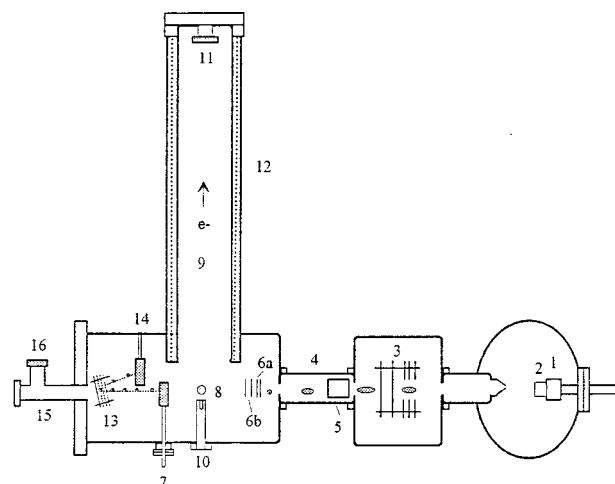


FIG. 2. The experimental system: Clusters are formed in an expansion through a pulsed supersonic nozzle (1) crossed by an electron source (2). Clusters are accelerated (3) into a flight tube (4) of a TOF mass spectrometer through an electrostatic lens (5). A mass gate-energy filter [6(a)] is followed by an impulse decelerator [6(b)], followed by a removable ion detector (7). A laser beam [perpendicular to the plane of the drawing] (8) intersects the ion beam and detaches electrons which are directed towards the solenoid drift tube (9) by a strong diverging magnetic field (10) and guided to the electron detector (11) by a low magnetic field produced by a solenoid coil (12). A reflectron mass spectrometer (13), coaxial with the ion beam, is used to detect (14) charged fragments. Fast neutral fragments are detected by a neutral detector (15, 16).

excited states of Γ^-Xe_n clusters. The current paper significantly expands the results of BMC. The size range of investigated Γ^-Xe_n clusters is extended to include second solvation layer effects ($n=1-54$). We investigate the autodetaching bound states relating to the $J=1/2$ spin state of the iodine core, and use two-photon action spectroscopy (2PAS) as well as neutral fragment spectroscopy in order to characterize the extended excited states. Altogether, these studies offer a comprehensive picture on the nature of the excited states in Γ^-Xe_n , in accordance with our initial assignment.¹³

II. EXPERIMENT

A scheme of the experimental setup is shown in Fig. 2. Negatively charged Γ^-Xe_n clusters are produced in the early stages of a supersonic expansion from a pulsed nozzle. The expanding gas consists of 3–4 bars mixture of 5% Xe in 95% Ar, passed through a cooled ($\approx -60^\circ\text{C}$) reservoir of methyl-iodide. The expansion is intersected by a 100–200 eV electron beam ending up in the formation of Γ^-Xe_n clusters. The newly formed clusters are cooled by a further flow in the expansion, and skimmed through a differentially pumped chamber to a chamber where they are mass-separated by a Wiley–McLaren time-of-flight mass spectrometer¹⁷ (TOFMS). The accelerated ions are directed by an electrostatic lens along a 1 m free-drift tube towards a microsphere plate (MSP®¹⁸) detector. The resolution of the mass spectrum, with a 1.8 cm-wide ion beam is $t/\Delta t \approx 350$. Typical spectra of Γ^-Xe_n clusters under two expansion conditions are shown in Fig. 3.

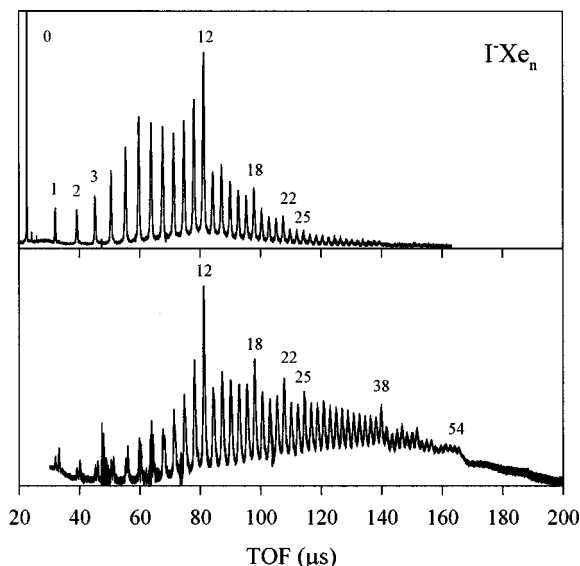


FIG. 3. Typical mass spectra of the I^-Xe_n clusters under two different expansion conditions. Note the magic numbers at $n=12, 18, 22, 25$, and 54. These numbers coincide with magic numbers in the mass spectra of positively charged Xe_n^+ clusters, if I^- is counted as well.

The weakly bound I^-Xe_n clusters tend to dissociate spontaneously during their flight. When spontaneous fragmentation occurs during drift in a Wiley–McLaren TOFMS, both the parent and the fragment ions share practically the same velocity (ignoring the small recoil energy gained in the fragmentation process). Each mass peak in the mass spectrum may consist of the parent ion as well as its fragment daughters. To minimize this effect in the spectroscopic studies of the mass-selected clusters, we have developed an energy-filter mass gate to remove the spontaneous fragments from the mass spectrum¹⁹ in which the intensity loss of the parent ion due to filtration is negligible. The effect of filtration is shown in Fig. 4.

Two sets of experiments are performed on the mass-selected cluster: PES for the determination of the EA, namely the energetics of the ground state, and energy-dependent photo-action spectroscopy for the characterization of the excited states.

A. Photoelectron spectroscopy

Our photoelectron spectrometer follows the design principles of Kruit and Read.²⁰ Our version is based on a “magnetic bottle” formed by a small pulsed solenoid (about 1 kG in the laser interaction zone), and a 1.67 meter guiding solenoid (~ 8 G).²¹ For $n < 8$, the clusters are decelerated before photodetachment by a voltage impulse, down to a low kinetic energy (≈ 30 eV) to reduce the Doppler-energy broadening of the photoelectron spectra.²² For larger clusters, this procedure is unnecessary due to their lower velocity.

The photoelectron spectra were taken with a photon energy that exceeded the energy of the neutral iodine $J=1/2$ spin state by ~ 0.5 eV. The spectrometer was calibrated with photoelectron spectra of I^- (Ref. 23) at the 4.66 eV photons of the Nd:YAG laser. A typical electron spectrometer energy resolution was ~ 60 meV at an electron energy of 1 eV.

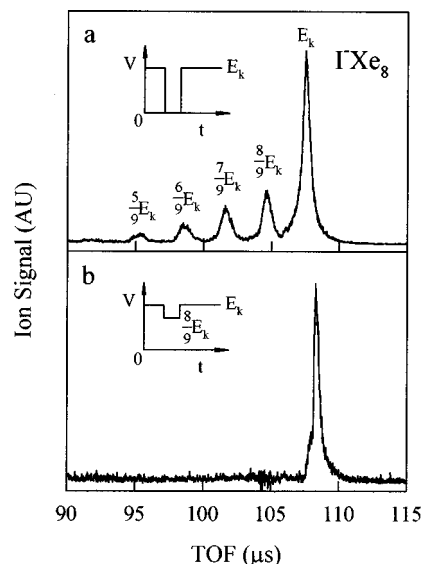


FIG. 4. A tandem reflectron mass spectrum of an I^-Xe_8 cluster, under relatively bad expansion conditions: (a) together with its daughters, selected by a conventional stopping MG, and (b) with no daughter peaks, selected by an energy-filter mass gate. Insets: The voltage pulsing on the conventional and energy-filter mass gates, respectively.

B. Action spectroscopy

The energy dependence of the photoinduced processes in the clusters was measured by using a tunable OPO laser system.²⁴ We have studied the photoexcitation process by monitoring the following products: electrons from single and two-photon excitations, photofragments, and fast neutral residues.

1. Electron ejection

We have measured the energy dependence yield of the photoelectrons below and above the vertical detachment threshold by slightly accelerating (0.5–2 eV) the electrons towards the detector. Two-photon photoelectron detachment was induced by overlapping the fundamental and the second harmonics of the tunable OPO laser system output.²⁴ The action spectra of the two-photon processes were taken by gating the appropriate higher-energy photoelectrons in the time-of-flight spectrometer.

2. Photofragmentation

Fragmentation could be a competing process to electron ejection. Charged fragments were monitored by a tandem coaxial Reflectron²⁵ TOFMS.²⁶ The resolution of our reflectron is $t/\Delta t \approx 700$ and we can observe distinct fragments which are 1% in quantity of their parent ion.

3. Neutral generation

In addition to action spectroscopy, in which electrons or photofragments are detected, one can monitor the yield of the fast neutral species generated in the former processes.²⁷ Although this detection scheme does not point directly to the occurring process, it has its distinct merits. Its signal is proportional to the total yield of the photo process, and it allows for the integration of the photo process over a microsecond

time scale after the excitation.²⁸ The key to efficient neutral detection is a high kinetic energy of the neutrals impinging on a high-efficiency electron ejection surface.²⁹ We have accelerated the charged clusters to about 5.5 keV prior to photoexcitation.

Spectra were acquired by a LeCroy 9310 transient recorder and transferred to the computer for event counting, data averaging, and processing.

III. RESULTS AND DISCUSSION

A. Mass spectrum and cluster temperature

Figure 3 shows the mass spectrum of $\text{I}^- \text{Xe}_n$, characterized by “magic numbers” typical to noble gas clusters, if I^- is counted as well. Particularly intense is the peak of $\text{I}^- \text{Xe}_{12}$. We anticipate this cluster to have an icosahedral structure with the I^- located in the center, symmetrically solvated by a shell of 12 xenon atoms. Other local magic numbers are $n=18, 22, 25,$ and 54 predicted by theoretical calculations for pure xenon clusters,³⁰ and coincide with experimental magic numbers of Xe_n^+ clusters.³¹ We speculate that the magic number at $n=38$ relates to a pack of three clusters: one is $\text{I}^- \text{Xe}_{12}$, and the other two are pure Xe_{13} icosahedrons.

We have used recent calculations of Jung and Gerber³² on the $\text{I}^- \text{Xe}_n$ system and the evaporative ensemble model³³ to evaluate the cluster temperature. Typical values are 80 and 40 K for the first and second solvation layer, respectively.

B. Photoelectron spectroscopy

Figure 5 displays photoelectron spectra of $\text{I}^- \text{Xe}_n$, $n=0-54$. All of these spectra are characterized by two peaks (about 0.95 eV apart), corresponding to the two J spin states ($J=1/2, 3/2$) of the neutral iodine core in the final state. We have assigned the peaks of these spectra to the vertical binding energies [$\text{VBE}_{3/2}(n)$ and $\text{VBE}_{1/2}(n)$, respectively] of the negatively charged clusters (Table I).

The difference between $\text{VBE}_{3/2}(n)$ and $\text{VBE}_{3/2}(0)$ (Table I), E_{stab} , represents mainly the stabilization of the ground state by the polarization interaction of the iodide with its xenon solvent. The size dependence of E_{stab} elucidates the evolution and grouping of xenon atoms around the main ion. Figure 6 presents E_{stab} as a function of the cluster size. Within our PES resolution, E_{stab} , as deduced from the $J=1/2$ final state [$\text{VBE}_{1/2}(n) - \text{VBE}_{1/2}(0)$], is identical. Note that the increase in E_{stab} in clusters containing more than 12 xenon atoms levels off dramatically. This is a strong indication that these 12 atoms form the first solvation shell around the ion. The addition of subsequent atoms to the second solvation layer involves smaller interactions with the ion, due to a larger distance. This curve, as well as the mass spectrum of Fig. 3, where $\text{I}^- \text{Xe}_{12}$ is a global magic number, supports the assignment of icosahedral structures to the $\text{I}^- \text{Xe}_n$ clusters.

C. Action spectroscopy - loosely bound excited states

As in BMC,¹³ we use the action spectra of electron detachment in order to identify the extended bound states in the $\text{I}^- \text{Xe}_n$ clusters. As previously emphasized, the current paper expands the scope of this study in two aspects: The size

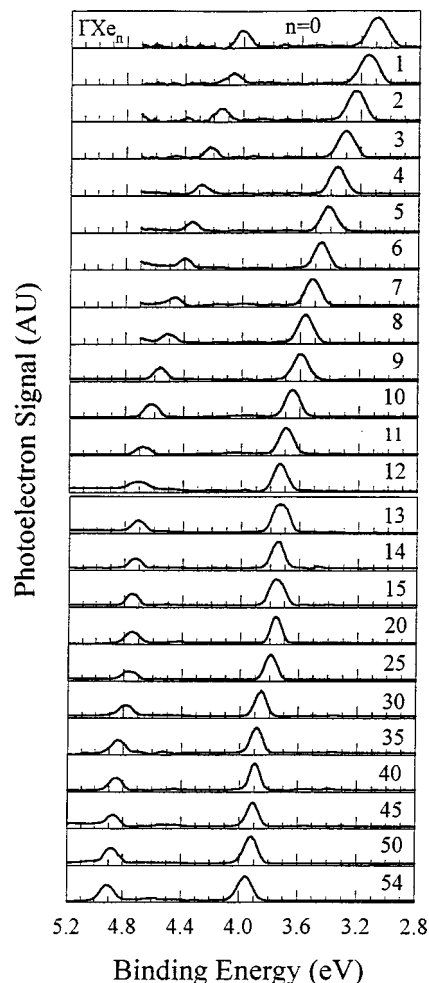


FIG. 5. Photoelectron spectra of the $\text{I}^- \text{Xe}_n$ clusters, $n=0-54$, taken using 5.01 eV and 5.27 eV photons.

range of the investigated $\text{I}^- \text{Xe}_n$ clusters is extended to include second solvation layer effects ($n=1-54$). The excitation energy range is expanded (3.0–4.95 eV) as well to include the autodetaching bound states relating to the $J=1/2$ continuum of the iodine core.

Figure 7 presents the action spectra for $\text{I}^- \text{Xe}_n$, $n=0-12$. No laser-induced fragmentation was observed for any of the above species, and electron emission was the exclusive decay channel. In Fig. 8, both the action spectrum and photoelectron spectrum of the $\text{I}^- \text{Xe}_{30}$ cluster are superimposed as an example of the relation between the photoelectron spectra and action spectra. The arrows in Fig. 7 mark the energies of the VBEs of the $J=3/2$ and $J=1/2$ states, respectively, as determined in our PES experiments.

Starting at $n \sim 4$, the following trends evolve with the cluster size:

- The very broad detachment spectrum of I^- , characteristic of localized to continuum transitions, narrows gradually to bands near and lower in energy than both $\text{VBE}_{3/2}(n)$ and $\text{VBE}_{1/2}(n)$.
- The relative cross section of absorption over the $J=3/2$ state grows gradually with the cluster size. Starting

TABLE I. Experimental binding energies, delocalization energies, and stabilization energies of iodide in I^-Xe_n clusters.

| N | VBE ^a at $J=3/2$ (eV) (± 30 meV) | VDE ^b at $J=3/2$ (eV) (± 3 meV) | Binding energy of excited electron ($J=3/2$)- V_0 (meV) (± 30 meV) | VBE ^a at $J=1/2$ (eV) (± 30 meV) | VDE ^b at $J=1/2$ (eV) (± 3 meV) | Binding energy of excited electron ($J=1/2$)- V_0 (meV) (± 30 meV) | E_{stab}^c (eV) |
|----|---|--|---|---|--|---|----------------------|
| 0 | 3.06 | ... | ... | 4.005 | ... | ... | |
| 1 | 3.13 | ... | ... | 4.076 | ... | ... | 0.07 |
| 2 | 3.22 | 3.255 | -35 | 4.166 | ... | ... | 0.16 |
| 3 | 3.29 | 3.295 | -5 | 4.236 | ... | ... | 0.23 |
| 4 | 3.35 | 3.339 | 11 | 4.296 | 4.261 | 32 | 0.29 |
| 5 | 3.41 | 3.391 | 19 | 4.356 | 4.308 | 48 | 0.35 |
| 6 | 3.46 | 3.440 | 20 | 4.406 | 4.354 | 52 | 0.40 |
| 7 | 3.51 | 3.486 | 24 | 4.456 | 4.400 | 56 | 0.45 |
| 8 | 3.56 | 3.532 | 28 | 4.506 | 4.441 | 65 | 0.50 |
| 9 | 3.60 | 3.569 | 31 | 4.546 | 4.470 | 76 | 0.54 |
| 10 | 3.65 | 3.608 | 42 | 4.596 | 4.515 | 81 | 0.59 |
| 11 | 3.69 | 3.641 | 49 | 4.636 | 4.552 | 85 | 0.63 |
| 12 | 3.73 | 3.675 | 55 | 4.666 | 4.576 | 90 | 0.67 |
| 13 | 3.746 | 3.678 | 68 | 4.692 | 4.592 | 100 | 0.686 |
| 14 | 3.754 | 3.684 | 70 | 4.700 | 4.596 | 104 | 0.694 |
| 15 | 3.763 | 3.690 | 73 | 4.706 | 4.606 | 110 | 0.703 |
| 20 | 3.793 | 3.712 | 81 | 4.739 | 4.616 | 123 | 0.733 |
| 25 | 3.810 | | | 4.756 | 4.626 | 130 | 0.750 |
| 30 | 3.848 | 3.757 | 91 | 4.794 | 4.658 | 136 | 0.788 |
| 35 | 3.869 | | | 4.815 | 4.676 | 139 | 0.809 |
| 40 | 3.894 | 3.787 | 107 | 4.840 | 4.690 | 150 | 0.834 |
| 45 | 3.914 | | | 4.860 | 4.704 | 156 | 0.854 |
| 50 | 3.935 | | | 4.881 | 4.719 | 162 | 0.875 |
| 54 | 3.955 | | | 4.901 | 4.731 | 170 | 0.895 |

^aVertical binding energy.^bVertical delocalization energy.^cStabilization energy.

from $n=1$, the peaks of the action spectra gradually increase by about two orders of magnitude³⁴ at $n=12$.

- (c) As the cluster grows, the peaks of the action spectra locate at an increasing energy spacing below the VBEs.

The above observations relating to both VBEs of the $J=3/2$ and $J=1/2$ states, reinforce the BMC identification of bound excited states lying below the $VBE_{3/2}$ in these clusters. We relate the excited-state bands to a transition from a localized electron state on the iodide to excited states on the

xenon solvent. We consider these transition energies to be the vertical delocalization energy ($VDE_{3/2}$ and $VDE_{1/2}$) of the iodide impurity.

The energy difference between the VBE and VDE may be negative or positive for bound and unbound delocalized states, respectively. These energy differences are the cluster equivalent of $-V_0$ in the bulk,³⁵ namely, the binding energy of the excess electron in the conduction band³⁶

$$VBE - VDE = -V_0. \quad (1)$$

In Table I, we summarize the values of VDE and $-V_0$ for both iodine spin states.

While the detachment of an electron excited above the $VBE_{3/2}$ may be a direct process, electron detachment below the $VBE_{3/2}$ is connected with cluster rearrangement. Following the vertical photoexcitation, vibrational relaxation processes in the excited state, as well as internal vibrational energy contained in the cluster prior to the photoexcitation, may raise the electron above its adiabatic binding energy (ABE). Consequently, electron detachment to the $J=3/2$ state occurs, in a process which is analogous to the bulk thermionic emission (TE).

TE was identified in anion clusters of two different types: Fullerenes³⁷ and refractory metals.³⁸ TE occurs as the major decay channel when other processes such as unimolecular dissociation and thermal radiation are slow. This requires a relatively high activation energy for the atomic

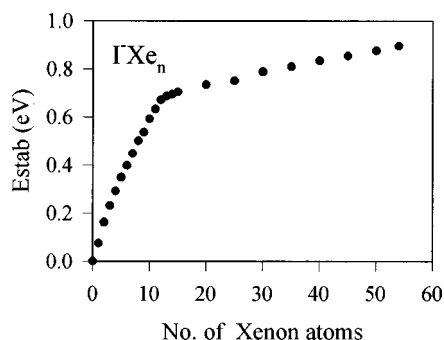


FIG. 6. The dependence of $E_{stab}(n) = VBE(n) - VBE(0)$ on the cluster size. Note that above $n=12$, E_{stab} levels off, indicating, that the first solvation layer around I^- consists of twelve xenon atoms.

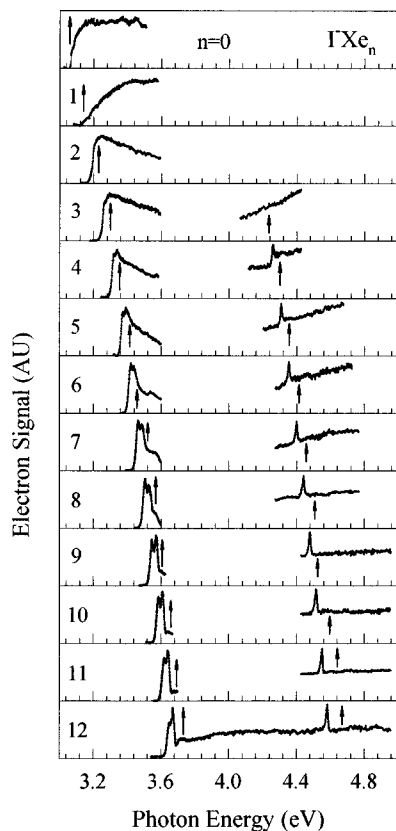


FIG. 7. Action spectra of the $\text{I}^- \text{Xe}_n$ clusters, for $n=0-12$. The arrows indicate the vertical binding energies (VBEs) of iodide with final $J=3/2$ and $J=1/2$ spin states of iodine.

evaporation in comparison to their EAs. According to our findings, the adiabatic EA of the clusters is lower than 50 meV, and the binding energy of a xenon atom at the first solvation shell is estimated by Jung and Gerber³² to be 4 kcal mol⁻¹ (=325 meV). Hence, the prevalence of the detachment process is intelligible.

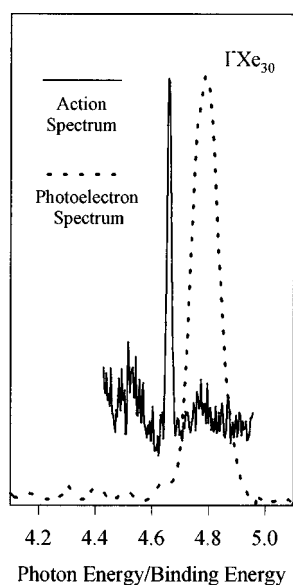


FIG. 8. Superposition of the action spectrum (solid line) and photoelectron spectrum (dotted line) of the $\text{I}^- \text{Xe}_{30}$ cluster.

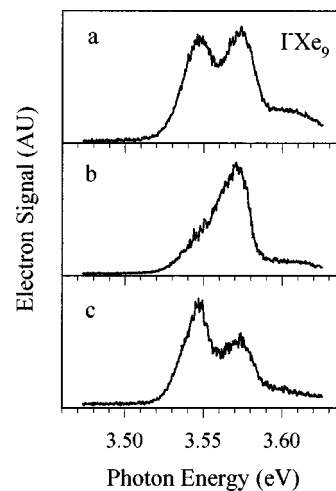


FIG. 9. The effect of nozzle temperature (T) and stagnation pressure (P) on the action spectra of $\text{I}^- \text{Xe}_9$: (a) $T=150^\circ\text{C}$, $P=4$ atm; (b) $T=150^\circ\text{C}$, $P=9$ atm; (c) $T=220^\circ\text{C}$, $P=4$ atm.

Electron ejection from excited bound states below the $J=1/2$ state, however, is simply autodetachment as the electron is coupled directly to the $J=3/2$ continuum. Note that the peaks that relate to the $J=1/2$ and $J=3/2$ continua are of comparable intensity. Since the final $J=1/2$ state is always coupled to a detachment continuum, one can deduce that the electron detachment probability is high also in the vicinity of the $J=3/2$ state at energies lying below the vacuum level.

The onset of the detachment of the action spectra at energies above the second ($J=1/2$) detachment continuum are puzzling to us. For the bare I^- (Ref. 39), two onsets appear in the action spectrum, which begin promptly at the threshold energies corresponding to the production of a free electron and an iodine atom at the $J=3/2$ and $J=1/2$ states. The shape of the onsets follow the ‘‘Wigner’’ threshold law⁴⁰ ($\sigma \propto (h\nu - \text{EA})^{l+1/2}$, where l is the angular momentum of the electron) for ejection of a p electron in iodide to an s wave continuum. Despite our expectations, no such onsets show in the spectra of $\text{I}^- \text{Xe}_n$ relating to the $J=1/2$ states. This phenomenon is probably induced by the presence of the xenon solvent. We find this observation outside the scope of the current work, and will not try to resolve it.

A distinct spectral splitting of ~ 20 meV shows in the action spectra starting from $\text{I}^- \text{Xe}_4$. Action spectra of the selected $\text{I}^- \text{Xe}_9$ cluster have been run at several nozzle-expansion conditions to clarify their nature. At higher stagnation pressures, which we associate with lower cluster temperature, the high-energy peak increased its relative intensity, while at higher nozzle temperature in the expansion, the low-energy peak was higher. These experimental findings are shown in Fig. 9. In BMC, we have attributed the splitting to hot bands in analogy to hot bands in the recent experiments on $\text{I}^- \text{Ar}_n$ clusters performed by Neumark and co-workers,¹⁶ accompanied by the calculations by Manolopoulos and co-workers.⁴¹ Since the peaks lying below the $J=1/2$ continuum are substantially narrower than the $J=3/2$ peaks and do not show any splitting, this assignment should be abandoned. The fact that only the states which refer to the $J=3/2$ continuum are split implies that the split-

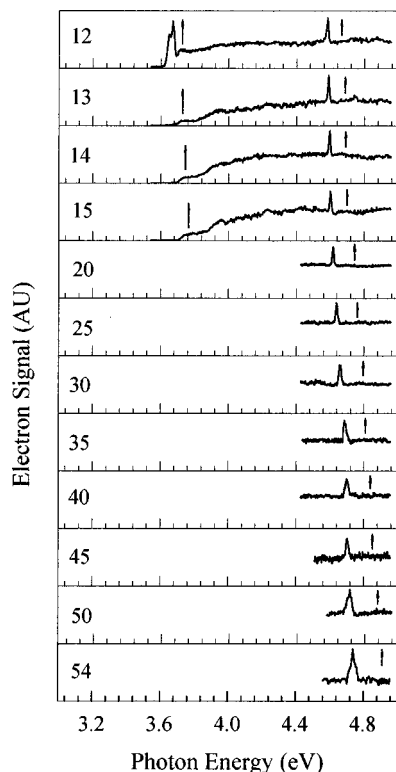


FIG. 10. Action spectra of the $\text{I}^- \text{Xe}_n$ clusters, for $n=12-54$. The arrows indicate the vertical binding energies (VBEs) of iodide with final $J=3/2$ and $J=1/2$ spin state of iodine.

ting originates from the degeneracy removal of the final $J=3/2$ state of the iodine core in the cluster.⁴² The temperature dependence of the relative intensities of the two peaks can be explained using the calculations of Jung and Gerber³² on the $\text{I}^- \text{Xe}_n$ system. They describe doublets (~ 24 meV spaced) in the photoelectron spectra of $\text{I}^- \text{Xe}_n$ in terms of a dynamic Jahn–Teller effect as the manifestation of the final $J=3/2$ nondegenerate states of the neutral iodine. According to these calculations, the temperature of the initial ground-state ion influences the ratio of the Franck–Condon overlap integral of the two nondegenerate $J=3/2$ states. Such splitting is not discerned in our photoelectron spectra due to their limited resolution. Since we assume that the bound excited states in our clusters are basically neutral core with a diffused bound electron, the analysis of the temperature dependence of the photoelectron spectra may apply to our experiment as well.

D. Action spectroscopy-strongly bound excited states

Starting at $n=13$, a dramatic change in the action spectra (Fig. 10) occurs. The peaks manifesting the existence of an excited state below the $J=1/2$ spin state still exist for *all* clusters. In contrast, the doublet peaks corresponding to $J=3/2$, which evolved and stabilized gradually up to $n=12$, abruptly *disappear* from the action spectra. Since the peak relating to the $J=1/2$ continuum develops regularly with cluster size, we believe in the existence of bound excited states also below the $J=3/2$ continuum. The disappearance of their spectral features from the electron detachment action

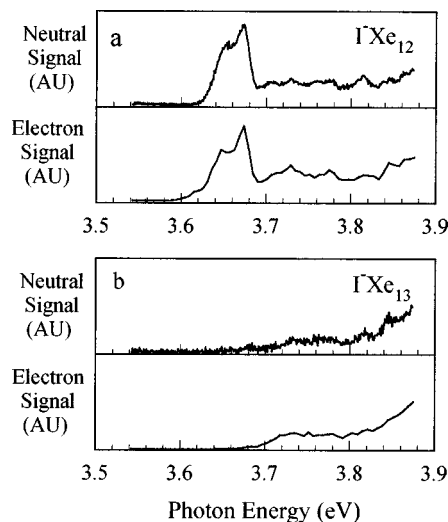


FIG. 11. A comparison between the neutral and the electron action spectra of (a) $\text{I}^- \text{Xe}_{12}$ and (b) $\text{I}^- \text{Xe}_{13}$. Note the resemblance between each pair of spectra which indicates that neutralization of the parent due to excitation results exclusively from electron emission.

spectrum could be attributed to the existence of a competing process to electron ejection, to slower electron ejection dynamics, or to the stabilization of the bound excited state. Accordingly, we have performed the following measurements:

- We considered a plausible photofragmentation of clusters for which $n > 12$, since the xenon binding energy of the second solvation layer is weaker than in the first solvation layer. No fragmentation was detected for $n = 13-15$ and 54.
- We have looked for electron ejection over a longer time scale than the time window of the magnetic bottle ($0.25 \mu\text{s}$ for $\text{I}^- \text{Xe}_{13}$), by performing fast neutral action spectroscopy. The time of flight of the parent ion to the neutral detector is about $40 \mu\text{s}$, allowing for the observation of electron detachment which is two orders of magnitude slower. Figure 11 compares electron spectra to neutral spectra of both $\text{I}^- \text{Xe}_{12}$ and $\text{I}^- \text{Xe}_{13}$. The identity between the neutral spectrum and the electron spectrum of each species proves that neutral production stems from electron ejection *only*. We did not reveal in the fast neutral action spectra any sign of a bound state related to the $J=3/2$ continuum.
- Finally, we have looked for the stabilization of the bound states related to $J=3/2$ by performing 2PAS. The second harmonics of the OPO was used to pump the excited state, while the fundamental was used to detach the excited bound electron. Only electrons with kinetic energy corresponding to these combined excitations were collected. Figure 12 presents the 2PAS spectra of $\text{I}^- \text{Xe}_n$ clusters, for $n > 12$. For $n < 12$, only an extremely weak 2PAS signal was detected. Note, in Fig. 12, the pattern resemblance of the 2PAS and the TE features of $\text{I}^- \text{Xe}_{12}$. It appears as if the TE features of the bound excited state switch over to the 2PAS for $n > 12$, indicating that at $n > 12$ the excited state is strongly stabilized, at least in the nanosecond time

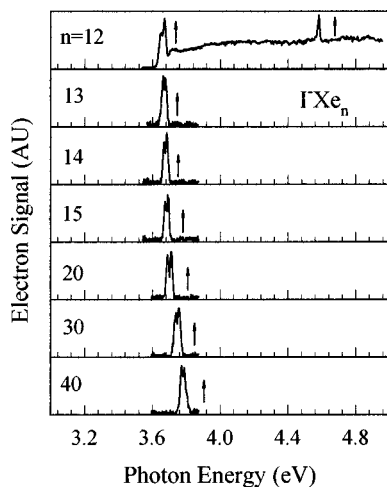


FIG. 12. The two-color, two-photon action spectra of the Γ^-Xe_n clusters, for $n=13-40$. The top panel includes the TE action spectrum of Γ^-Xe_{12} , for comparison. The arrows indicate the VBEs of iodide with final $J=3/2$ and $J=1/2$ spin state of iodine. Note the pattern resemblance of the 2PAS features and the TE features of Γ^-Xe_{12} .

scale. This stabilization inhibits TE over the time scale of the experiment, and in parallel, allows for a nano-second 2PAS. One needs, however, to explain the abrupt cluster-size transition in the disappearance of the TE and the appearance of the 2PAS signals.

The key parameter to this phenomenon is the size dependence of the cluster temperature. In the framework of the evaporative ensemble model,³³ the temperature of the cluster is determined by the dissociation energy of its weakest-bound component. The binding energy of the second-layer xenon atom is substantially lower than the binding energy of the 12th xenon atom in the first solvation layer. Consequently, the temperature of Γ^-Xe_n ($n>12$) is substantially lower. According to Gerber and Jung,³² the average binding energy of a xenon atom to the central iodide in the first solvation shell is approximately 4 kcal mol^{-1} , but only $1.9 \text{ kcal mol}^{-1}$ in the second solvation shell. The outcome of this lower temperature is that although the absolute value of V_0 gradually grows with cluster size, the lower temperature for $n>12$ slows TE down quite abruptly at this size. To emphasize this point, we present in Fig. 13 the electron TOF spectra of selected clusters, each taken at the action spectrum peak of the bound state related to the $J=3/2$ continuum. These spectra contain the contributions of both one-photon and two-photon detachments. Note that on ascending from Γ^-Xe_{12} to Γ^-Xe_{13} , the two-photon signals increase abruptly, at the expense of the one-photon signal, while for larger clusters, the dominance of the two-photon signal grows gradually, with the increase of binding energy ($-V_0$).

E. Comparison with calculations

Our motivation to perform the experiments was to study a model system that would mimic in its excited state the interaction of pure xenon clusters with excess electrons. We relate the excited-state bands to a transition from a localized electronic state on the iodide to excited states on the xenon

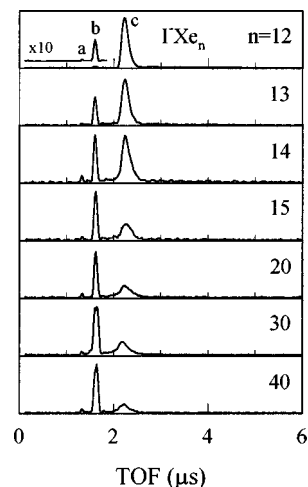


FIG. 13. A slightly accelerated ($\sim 100 \text{ meV}$) electron TOF spectra of selected Γ^-Xe_n clusters taken at photon energies of the action spectrum peaks related to the $J=3/2$ continuum. Note the changing ratio between the one-color, two-photon (a), two-color, two-photon (b), and the TE (c) signals.

cluster. We believe the binding energy values, which we assign to $-V_0$, to be analogous to the binding energies of an electron to ground-state Xe_n^- clusters. In Fig. 14, we compare our measured $-V_0$ values with the theoretical diffusion Monte Carlo simulation results of Martyna and Berne¹¹ on Xe_n^- and the continuum approximation of Stampfli and Bennemann.¹² Clearly, we expect no match at the limit of small clusters, since the effect of the neutral iodine on the electron binding energy may be substantially larger than that of atomic xenon.⁴³ Based on this fact, we wish to study the incremental stabilization of the excited electron with the addition of xenon atoms. It seems that in the first solvation layer, the incremental stabilization in our experiments grows twice as much as that of the calculations ($\sim 6 \text{ meV}$ per xenon atom in the experiment vs $\sim 2.6 \text{ meV}$ in the calculations of Martyna and Berne¹¹). This effect may result from the difference between our model system and the simulated pure xenon clusters, yet it may indicate some fault in the calculations of the small clusters. In contrast, in the larger cluster

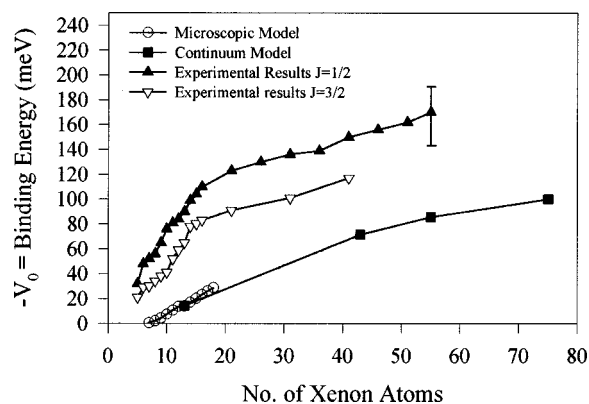


FIG. 14. Our experimental $-V_0$ values of the Γ^-Xe_n clusters (full and open triangles) compared to the calculated binding energy of the excess electron at the ground state of Xe_n^- clusters: diffusion Monte Carlo simulations of Ref. 11 (open circles) and the continuum approximation of Ref. 12 (full squares).

range ($n = 13-54$) the differential stabilization practically coincides with the calculations¹² (~ 1.44 vs 1.41 meV in the experiments and the calculations, respectively).

IV. CONCLUSIONS

The picture which was unveiled from the above photoelectron and action spectra (TE and 2PAS) is the gradual evolution of bound excited states on the xenon solvent cluster. As the clusters grow, their binding energy increases. In parallel, the loosely bound excited states, which extend beyond the cluster size,¹¹ shrink and gain oscillator strength. This is due to better electronic overlaps with the localized ground state, at the expense of the transitions to the vacuum. Such behavior is typical for Rydberg states as well as other loosely bound electronic states in clusters, such as solvated excess electrons^{6,7,44,45} and dipole bound⁴⁶ states.

The existence of the bound states has been established for both spin states of the neutral iodine core, either by TE, autodetachment, or by two-photon experiments. The onset of the 2PAS features on the nanosecond time scale at $n > 12$ for the $J = 3/2$ related states, which evolve gradually in energy as a smooth continuation of the TE signals, reinforces our assignment of the TE peaks in the small I^-Xe_n ($n < 12$) clusters as bound delocalized excited states.

The width of the $J = 1/2$ related excited state action spectrum feature is ca. 20 meV. In terms of time, it is equivalent to 0.5 ps. This number sets the lower limit for the lifetime of these clusters. An upper limit for the lifetime cannot be given, since it is a one-photon experiment. As for the $J = 3/2$ related excited state that is probed using a two-photon process (starting from $n = 13$), one can conclude that the lifetime is of the order of the pulse width, in the nanosecond range. The above limits clearly indicate that the I^-Xe_n cluster system exhibits interesting electron dynamics that can be probed using a femtosecond laser.

ACKNOWLEDGMENTS

The research was supported by the James Franck German-Israeli Binational Program in Laser Matter Interactions, by the US-Israel Binational Foundation, and by The Israel Science Foundation founded by the Israel Academy of Sciences and Humanities. We wish to thank R. Giniger and Y. Magen for technical help, and J. Jortner, R. B. Gerber, U. Even and W. Christen for useful discussions.

¹L. Kevan, J. Phys. Chem. **76**, 3830 (1972); B. Baron, D. Hoover, and F. Williams, J. Chem. Phys. **68**, 1997 (1978).

²W. von Zdrojewski, J. G. Rabe, and W. F. Schmidt, Z. Naturforsch. A **35A**, 672 (1980); R. Reininger, U. Asaf, and I. T. Steinberger, Chem. Phys. Lett. **90**, 287 (1982).

³M. Knapp, O. Echt, D. Kreisler, T. D. Mark, and E. Recknagel, in *Physics and Chemistry of Small Clusters*, edited by P. Jena, B. K. Rao, and S. N. Khanna (Plenum, New York, 1987), p. 693.

⁴M. J. Deluca, B. Niu, and M. A. Johnson, J. Chem. Phys. **88**, 5857 (1988).

⁵S. H. Fleischman and K. D. Jordan, J. Phys. Chem. **91**, 1300 (1987).

⁶H. Haberland, C. Ludewigt, H. G. Schindler, and D. R. Worsnop, Surf. Sci. **156**, 157 (1985); G. H. Lee, S. T. Arnold, J. G. Eaton, H. W. Sarkas, K. H. Bowen, C. Ludewigt, and H. Haberland, Z. Phys. D **20**, 9 (1991).

⁷H. Haberland, C. Ludewigt, H. G. Schindler, and D. R. Worsnop, Phys. Rev. A **36**, 967 (1987); J. V. Coe, G. H. Lee, J. G. Eaton, S. T. Arnold, H. W. Sarkas, K. H. Bowen, C. Ludewigt, H. Haberland, and D. R. Worsnop, J. Chem. Phys. **92**, 3980 (1990).

⁸J. Gspann, Physica B **169**, 519 (1991); T. Jiang, C. Kim, and T. A. Northby, Phys. Rev. Lett. **71**, 700 (1993); U. Henne and J. P. Toennies, J. Chem. Phys. **108**, 9327 (1998).

⁹K. Martini, J. P. Toennies, and C. Winkler, Chem. Phys. Lett. **178**, 429 (1991).

¹⁰H. Haberland, T. Kolar, and T. Reiners, Phys. Rev. Lett. **63**, 1219 (1989).

¹¹G. J. Martyna and B. J. Berne, J. Chem. Phys. **88**, 4516 (1988); **90**, 3744 (1989).

¹²P. Stampfli and K. H. Bennemann, Phys. Rev. A **38**, 4431 (1988); Z. Phys. D **20**, 53 (1991).

¹³I. Becker, G. Markovich, and O. Cheshnovsky, Phys. Rev. Lett. **79**, 3391 (1997).

¹⁴One may argue that I^-Xe_n should be compared to Xe_{n+1}^- because then, the number of polarizable species (including the iodine core) is equal. As the binding energy increases monotonically, such a distinction is of minor importance.

¹⁵S. T. Arnold, J. H. Hendricks, and K. H. Bowen, J. Chem. Phys. **102**, 39 (1995).

¹⁶Y. Zhao, I. Yourshaw, G. Reiser, C. C. Arnold, and D. M. Neumark, J. Chem. Phys. **101**, 6538 (1994); I. Yourshaw, Y. Zhao, and D. M. Neumark, *ibid.* **105**, 351 (1996).

¹⁷W. C. Wiley and I. H. McLaren, Rev. Sci. Instrum. **26**, 1150 (1955).

¹⁸El-Mul Technologies Ltd., Israel.

¹⁹I. Becker and O. Cheshnovsky, Rev. Sci. Instrum. **68**, 4625 (1997).

²⁰P. Kruit and F. H. Read, J. Phys. E **16**, 313 (1983).

²¹O. Cheshnovsky, S. H. Yang, C. L. Pettiette, M. J. Craycraft, and R. E. Smalley, Rev. Sci. Instrum. **58**, 2131 (1987).

²²G. Markovich, S. Pollack, R. Giniger, and O. Cheshnovsky, J. Chem. Phys. **101**, 9344 (1994).

²³H. Hotop and W. C. Lineberger, J. Phys. Chem. Ref. Data **4**, 539 (1975).

²⁴A Continuum Sunlite® OPO and FX-1 doubler pumped by a Continuum Powerlite® Nd:YAG.

²⁵V. I. Karataev, B. A. Mamyurin, and D. V. Shmikk, Sov. Phys. Tech. Phys. **16**, 1177 (1972); B. A. Mamyurin, V. I. Karataev, D. V. Shmikk, and V. A. Zagulin, Sov. Phys. JETP **37**, 45 (1973).

²⁶M. L. Alexander, N. E. Levinger, M. A. Johnson, D. Ray, and W. C. Lineberger, J. Chem. Phys. **88**, 6200 (1988).

²⁷M. A. Johnson and C. W. Lineberger, in *Techniques in Chemistry* (Wiley, New York, 1982), Vol. 20, p. 591.

²⁸In contrast, conventional electron ejection and fragment detection are restricted to the nanosecond time scale.

²⁹D. Bahatt, O. Cheshnovsky, U. Even, N. Lavie, and Y. Magen, J. Phys. Chem. **91**, 2460 (1987).

³⁰M. R. Hoare and P. Pal, Adv. Phys. **20**, 161 (1971).

³¹J. Farges, M. F. De Faraudy, B. Raoult, and G. Torchet, Surf. Sci. **156**, 370 (1985).

³²J. Jung, P. Jungwirth, and R. B. Gerber (unpublished).

³³C. E. Klots, J. Chem. Phys. **83**, 5854 (1985); C. E. Klots, Nature (London) **327**, 222 (1987).

³⁴The peak intensities were normalized to the ion signal; however, the detection sensitivity of ion detection as a function of cluster size was not calibrated.

³⁵J. Jortner and A. Gaaton, Can. J. Chem. **55**, 1801 (1977).

³⁶In Ref. 13, we have erroneously assigned this difference as V_0 , which is contrary to the convention of assigning negative values of V_0 to bound states.

³⁷K. Hansen and O. Echt, Phys. Rev. Lett. **78**, 2337 (1997); A. Bekkerman, B. Tsipinyk, A. Budervhich, and E. Kolodney, J. Chem. Phys. **108**, 5165 (1998).

³⁸H. Weidle, D. Kreisler, E. Recknagel, G. Schulze Icking-Konert, H. Handschuh, G. Gantefor, and W. Eberhardt, J. Chem. Phys. **237**, 425 (1995).

³⁹D. Serxner, C. E. H. Dessent, and M. A. Johnson, J. Chem. Phys. **105**, 7231 (1996).

⁴⁰E. P. Wigner, Phys. Rev. **73**, 1002 (1948).

⁴¹M. L. Brewer, J. S. Hulme, and D. E. Manolopoulos, J. Chem. Phys. **106**, 4832 (1997).

⁴²We thank the anonymous referee of Ref. 13 for suggesting the interpretation of degeneracy removal.

⁴³i.e., the atomic polarizability of I ($5.35A^3$) is bigger than that of Xe ($4.04A^3$).

⁴⁴R. N. Barnett, U. Landman, D. Scharf, and J. Jortner, *Acc. Chem. Res.* **22**, 350 (1989); Y. A. Yang, L. A. Bloomfield, C. Jin, L. S. Wang, and R. E. Smalley, *J. Chem. Phys.* **96**, 2453 (1992).

⁴⁵P. J. Campagnola, D. J. Lavrich, M. J. Deluca, and M. A. Johnson, *J. Chem. Phys.* **94**, 5240 (1991); P. Ayotte and M. A. Johnson, *ibid.* **106**, 811 (1997).

⁴⁶C. Desfrancois, H. Abdoul-Carime, and J.-P. Schermann, *Int. J. Mod. Phys. B* **10**, 1339 (1996).